Ocean Engng, Vol. 20, No 6, pp. 569–599, 1993.
Printed in Great Britain.

0029–8018/93 $6.00 + .00
Pergamon Press Ltd

DRAG-INDUCED INSTABILITIES AND CHAOS IN MOORING SYSTEMS

O. GOTTLIEB* and S. C. S. YIM†

*Ralph M. Parsons Laboratory, Department of Civil Engineering, Massachusetts Institute of Technology, Cambridge, MA 02139, U.S.A.; †Ocean Engineering Program, Department of Civil Engineering, Oregon State University, Corvallis, OR 97331-2302, U.S.A.

Abstract—The influence of a quadratic viscous drag nonlinearity in multi-point mooring systems is examined in this paper. These systems are characterized by a nonlinear restoring force and a coupled wave–structure exciting force. Stability analysis of system response and its corresponding Poincaré map define domains of primary and subharmonic resonances and reveal the existence of coexisting nonlinear solutions. Local and global tangent and period doubling bifurcations identify possible routes to chaotic motion and their controlling parameters. Thus, complex dynamics are obtained semi-analytically resulting in identification and control of the drag-induced instabilities which are not attainable by equivalently linearizing the hydrodynamic drag force.

1. INTRODUCTION

COMPLEX nonlinear and chaotic responses have been recently observed in various numerical models of compliant ocean systems (e.g. Thompson *et al.*, 1984; Papoulias and Bernitsas, 1988; Bishop and Virgin, 1988; Sharma *et al.*, 1988; Bernitsas and Chung, 1990; Choi and Lou, 1991; Jiang, 1991; Gottlieb and Yim, 1992). These systems are generally characterized by a nonlinear structural mooring force and a nonlinear hydrodynamic exciting force. The mooring force, which includes material discontinuities and geometric nonlinearities associated with mooring line angles, has a unique equilibrium position which is described by a single potential well. The exciting force consists of a quadratic wave–structure drag component and a harmonic wave-induced inertial force.

While weakly nonlinear systems have been studied extensively from both classical (Nayfeh and Mook, 1979) and modern approaches (Guckenheimer and Holmes, 1986), complex single equilibrium point systems with a strong nonlinearity are limited in their scope of analysis. Examples of these systems are the hardening Duffing equation analyzed by modified multiple scales (Rahman and Burton, 1986) and by the method of harmonic balance (Szemplinska-Stupnika, 1987) and the subharmonic motions of a wind-loaded structure analyzed by the general method of averaging (Holmes, 1980). Stability analysis of system behavior results in bifurcation maps defining regions of existence of various nonlinear phenomena in parameter space. This analysis can be performed by directly perturbing an approximate system solution or by evaluating the stability of the corresponding Poincaré map. Stability of the map's fixed points correspond to stability of the system's limit cycles (Wiggins, 1990). Perturbation of an approximate solution yields a nonlinear variational system which can be linearized to obtain a generalized Hill's system. Stability of the variational system can be obtained

numerically by Floquet analysis (Ioos and Joseph, 1981) or by analytically solving the Hill's equation (Hayashi, 1964).

Mooring system models which have been investigated to date (e.g. above-noted references) can be described by two categories. The first consists of models in which the nonlinear hydrodynamic exciting force is simplified in order to enable analysis of the highly nonlinear mooring restoring force. A characteristic example is a single degree-of-freedom harmonically excited nonlinear mooring oscillator. This oscillator includes a nonlinear function describing the mooring restoring force, whereas the nonlinear drag force is equivalently linearized (e.g. Bishop and Virgin, 1988; Choi and Lou, 1991). The second category consists of models incorporating both structural and hydrodynamic nonlinearities. A characteristic example is a quasi-static multi-degree-of-freedom single and two point mooring system subjected to steady (Bernitsas and Chung, 1990) and time varying (Jiang and Schellin, 1989) excitations. In this complex model the nonlinear viscous drag force was also linearized and combined with the structural damping associated with the mooring system. Other examples are the analysis of a quintic polynomial derived for the restoring moment of a rolling ship where the quadratic damping moment was linearized (Witz *et al.*, 1989) or approximated by a mixed linear-cubic model (Nayfeh and Khdeir, 1986).

These models exhibit a variety of nonlinear and chaotic phenomena but due to their complexity, identification and control of the mechanisms generating the nonlinear stabilities are not always attainable. Furthermore, models employing equivalent linearization of the hydrodynamic viscous drag force are valid for unbiased, small amplitude system response whereas many of the drag-induced instabilities are generated by near resonant phenomena where the resultant response is not small. Examples of the influence of the nonlinear drag on various ocean systems can be found in the numerical analysis of a harmonically excited linearized mooring system (Liaw, 1988) and in the semi-analytical analyses of a nonlinear mooring system (Gottlieb, 1991), a wave–structure interaction system (Gottlieb, 1992) and of a free floating articulated tower (Gottlieb *et al.*, 1992).

This paper describes the influence of the quadratic viscous drag nonlinearity on a nonlinear ocean system with a taut symmetric variable mooring assembly. In order to consistently model the nonlinear wave–structure coupling effect, the exact quadratic drag component is retained and not approximated. Section 2 describes the model formulation and identification of drag-induced system instabilities. In Section 3, global stability of the weakly excited system is demonstrated by a Liapunov function approach and stability of near resonant primary and subharmonic solutions is investigated by construction and analysis of the Poincaré map. Existence of period doubling is shown in Section 4, and Section 5 describes the evolution of local and global tangent and period doubling bifurcations and possible routes to chaotic motion. We conclude with some closing remarks.

2. SYSTEM MODEL

The mooring system considered (Fig. 1) is modeled as a single degree-of-freedom, hydrodynamically damped and excited nonlinear oscillator (surge). The equation of motion includes a symmetric geometrically nonlinear restoring force and an exciting force modeled by a relative motion Morison equation. The exciting force, which includes

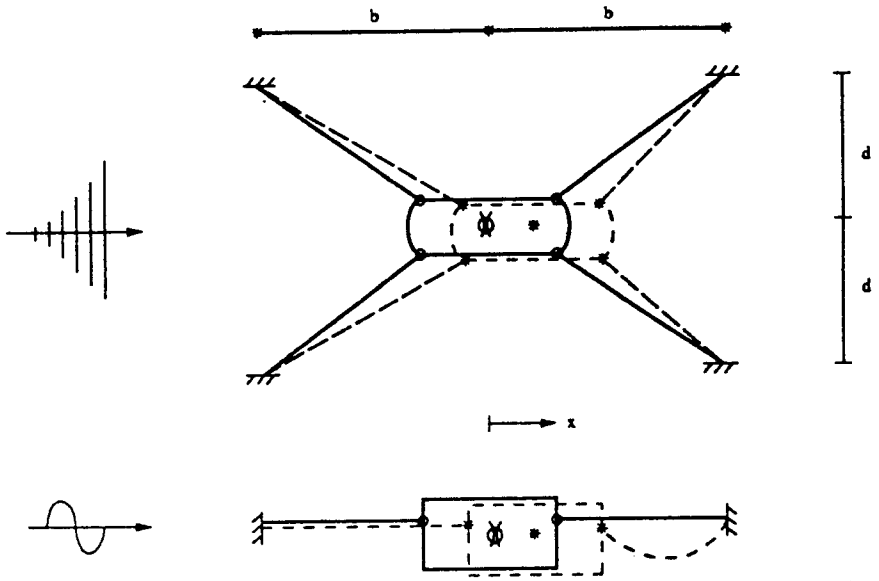

FIG. 1. Mooring assembly.

a quadratic coupled drag component and a harmonic inertial component, is derived based on small body motion under small amplitude wave excitation (Sarpkaya and Isaacson, 1981).

2.1. *Model formulation*

The restoring force (R) contains a strong geometric nonlinearity depending on the magnitude of the mooring angle. The degree of nonlinearity can vary from a highly nonlinear two-point mooring system ($b = 0$) to an almost linear four-point system ($b \gg d$).

The exciting force consists of a drag component (F_D) and an inertial component (F_I) with frequency independent coefficients. It is derived based on small body theory which assumes that the presence of the structure does not affect the wave field, hence waves propagating past the structure remain unmodified. This approach can be justified for slender body motion in the vertical plane (surge, heave, pitch) where the wavelength is large compared to the beam of the structure (Newman, 1977):

$$M\ddot{X} + C\dot{X} + R(X) = F_D(\dot{X},t) + F_I(\ddot{X},t) \tag{1a}$$

where

$$R = K[X + sgn(X)b]\left\{1 - \sqrt{\frac{d^2 + b^2}{d^2 + [X + sgn(X)b]^2}}\right\} \tag{1b}$$

$$F_D = \frac{1}{2}\rho A_p C_d (U - \dot{X})|U - \dot{X}| \tag{1c}$$

$$F_I = \rho \forall (1 + C_a)\left[\frac{\partial U}{\partial t}\right] - \rho \forall C_a \ddot{X} \tag{1d}$$

$$U = \omega a U_1 \cos(\omega t) \tag{1e}$$

and

M, C, K—system mass, structural damping and stiffness [$K = 2EA_c / \sqrt{(d^2+b^2)}$, EA_c elastic cable force].
a, ω, k—wave amplitude, frequency and number [$\omega^2 = gk \tanh kh$].
ρ, g, h—water mass density, gravitational acceleration and water depth.
A_p, $\forall$—projected drag area and displaced volume.
C_d, C_a—hydrodynamic viscous drag and added mass coefficients.
U_1—depth (z) parameter [$U_1 = \cosh k(z+h)/\sinh(kh)$].

Note that ($\dot{}$) is differentiation with respect to time and $sgn(X)$ denotes the sign of X.

The expansion of the restoring force in a least-square sense yields an odd polynomial. Rearranging and normalizing the equation of motion [Equation (1)] results in the following first order autonomous system ($x = kX$, $\theta = \omega t$):

$$\begin{aligned} \dot{x} &= y \\ \dot{y} &= -R(x) - \gamma y + F_D(y,\theta) + F_I(\theta) \\ \dot{\theta} &= \omega \end{aligned} \tag{2a}$$

where

$$R(x) = \sum_n \alpha_n x^n; \quad n = 1, 3, 5, \ldots, N \tag{2b}$$

$$F_D(y,\theta) = \mu \delta\left(f\cos\theta - \frac{y}{\omega}\right)\left|f\cos\theta - \frac{y}{\omega}\right| \tag{2c}$$

$$F_I(\theta) = -\mu \omega^2 f \sin\theta \tag{2d}$$

and

$$\alpha_n = \frac{K_n}{M+\rho\forall C_a}; \quad K_n = K_n(K,kb,kd)$$

$$\gamma = \frac{C}{M+\rho\forall C_a}$$

$$\delta = \frac{1}{2}\frac{C_d A_p}{(1+C_a)\forall} g \tanh kh$$

$$\mu = \frac{\rho\forall(1+C_a)}{M+\rho\forall C_a}$$

$$f = k a U_1.$$

Note the following limiting bounds on the mass (μ), viscous drag (δ), structural

damping (γ) and wave forcing (f) parameters: $\mu \geq 1$ (buoyancy), $\delta < 1$, $\gamma \ll 1$, $f < 1$ [$ka < \pi/7$ (limiting wave steepness), $U_1 \leq 1$ ($kh > \pi/10$ deep water)].

2.2. *Identification of nonlinearities*

The geometrically nonlinear restoring force is described by an odd polynomial function where the degree of nonlinearity is characterized by the magnitude of the amplitudes (α_n). The highly nonlinear two-point mooring system ($b = 0$) is found to be without a linear term ($\alpha_1 = 0$) whereas the weakly nonlinear four-point system is described with decreasing coefficients and is limited by a linearized mooring configuration ($\alpha_1 = 1$, $\alpha_{n>1} = 0$) corresponding to very small mooring line angles. The quadratic drag nonlinearity consists of a bias [$1/2\mu\delta f^2$], a harmonic exciting component [$1/2\mu\delta f^2 \cos 2\theta$], a parametrically excited term [$\mu\delta f \cos\theta\ (y/\omega)$] and a quadratic damping term [$\mu\delta\ (y/\omega)^2$].

The governing system nonlinearities ($N = 3$) are quadratic (y^2) and cubic (x^3) and the system is subjected to both parametric and external excitation complemented by a weak bias. Comparison of weakly nonlinear quadratic and equivalently linearized damping functions (e.g. Nayfeh and Mook, 1979) reveals that their rate of decay is proportional to the square of the amplitude of the initial disturbance and to the amplitude itself, respectively. A bias and parametric excitation in weakly nonlinear dynamical systems have been found to be a precursor for symmetry breaking leading to period doubling and a generating mechanism for system instabilities even for small amplitude response (e.g. Salam and Sastry, 1985; Miles, 1988). Thus, instabilities and chaotic motion in nonlinear ocean mooring systems would appear structurally different in systems excited by a coupled fluid–structure quadratic drag force vs that excited by an equivalently linearized drag force. Furthermore, even linearized mooring systems subjected to nonlinear viscous effects will retain the quadratic nonlinearity, bias and combined parametric and external excitation.

3. STABILITY ANALYSIS AND THE POINCARÉ MAP

Global stability of the multi-point mooring system was demonstrated in earlier work by a Liapunov function approach (Gottlieb and Yim, 1991) for very small excitation and small amplitude response. A weak Liapunov function [$L(x,y)$] was found for the unforced ($f = 0$), undamped ($\gamma,\delta = 0$) Hamiltonian system [$L(x,y) = y^2/2 + V(x)$ where $V(x) = \int R(x)dx$]. Thus, the origin [$(x,y)_e = (0,0)$] was found neutrally stable [$L(0,0) = 0$ and $dL/dt \equiv 0$]. Modification of $L(x,y)$ to account for structural damping (γ) and the choice of a sufficiently small parameter (ν: $0 < \nu < \gamma$), revealed a globally stable unforced system [$L(x,y)$ positive definite and $dL/dt \leq 0$].

$$L(x,y) = \frac{1}{2}y^2 + V(x) + \nu(xy + \frac{1}{2}\gamma x^2) \tag{3a}$$

$$\dot{L}(x,y) = -\nu[xR(x)] - (\gamma - \nu)y^2 . \tag{3b}$$

This strong Liapunov function describes in phase plane (x,y) an asymptotically stable hyperbolic fixed point (sink) at the origin. With the addition of wave excitation, the sink becomes a hyperbolic closed orbit (limit cycle). Although the stable limit cycle loses the circularity of the sink, it is anticipated by the invariant manifold theorem to

retain its stable characteristics (Guckenheimer and Holmes, 1986). While this result ensures that solutions will remain bounded for very small excitation ($|F_D|$, $|F_I| \ll 1$), it does not apply to system response with larger excitation or address the coexistence of nonlinear solutions and their sensitivity to initial conditions. Therefore, local analysis (in phase space) is required in order to investigate system stability for larger motion. This is achieved by analyzing the stability of the Poincaré map obtained by characterization of the fixed points of the averaged system which in turn correspond to near resonance solutions of the system itself.

3.1. *Averaging and the Poincaré map*

In order to evaluate the stability of system response under larger excitation, it is convenient to consider system response in the context of the Poincaré map where the solution is stroboscopically sampled at each forcing period ($T = 2\pi/\omega$). By employing the averaging theorem (Sanders and Verhulst, 1985), hyperbolic fixed points of the averaged system will correspond to periodic orbits of the forcing period. This can be demonstrated by use of the following invertible van der Pol transformation where $\mathbf{q} = (x,y)^T$ is periodic in t with period $2\pi m/\omega$, where m is the order of the subharmonic ($m = 1,2,3, \ldots, M$).

$$\begin{pmatrix} u \\ v \end{pmatrix} = A \begin{pmatrix} x \\ y \end{pmatrix} \tag{4a}$$

where

$$A = \begin{pmatrix} \cos\frac{\theta}{m} & -\frac{m}{\omega}\sin\frac{\theta}{m} \\ -\sin\frac{\theta}{m} & -\frac{m}{\omega}\cos\frac{\theta}{m} \end{pmatrix} \tag{4b}$$

and

$$A^{-1} = \begin{pmatrix} \cos\frac{\theta}{m} & -\sin\frac{\theta}{m} \\ -\frac{\omega}{m}\sin\frac{\theta}{m} & -\frac{\omega}{m}\cos\frac{\theta}{m} \end{pmatrix}. \tag{4c}$$

Thus, the fixed point of the averaged system corresponds to a period m point of the Poincaré map corresponding to a subharmonic of order m in the system (Wiggins, 1990).

We prepare our system [Equation (2)] for averaging by rewriting the system in the standard form: $d\mathbf{q}/dt = \mathbf{F}(\mathbf{q}) + \epsilon\mathbf{G}(\mathbf{q})$ where $\epsilon << 1$ [$\mathbf{F} = (F_1(\mathbf{q}),F_2(\mathbf{q}))^T$, $\mathbf{G} = (G_1(\mathbf{q},\theta),G_2(\mathbf{q},\theta))^T$] and by defining a detuning parameter $\epsilon\,\Omega = \omega^2 - m^2\alpha_1$ denoting nearness to primary ($m = 1$) and subharmonic ($m > 1$) resonances. Applying the van der Pol transformation [Equation (4)] to the system [Equation (2)] results in the following:

$$\begin{pmatrix}\dot{u}\\ \dot{v}\end{pmatrix} = -\frac{\epsilon}{m\omega}\left[R(u,v,\theta) + C(u,v,\theta) + F_D(u,v,\theta) + F_I(\theta)\right]\begin{pmatrix}\sin\frac{\theta}{m}\\ \cos\frac{\theta}{m}\end{pmatrix} \tag{5a}$$

where

$$R(u,v,\theta) = \Omega\left(u\cos\frac{\theta}{m} - v\sin\frac{\theta}{m}\right) - m^2\sum_{n+2}\alpha'_n\left(u\cos\frac{\theta}{m} - v\sin\frac{\theta}{m}\right)^{n+2} \tag{5b}$$

$$C(u,v,\theta) = m\omega\gamma'\left(u\sin\frac{\theta}{m} + v\cos\frac{\theta}{m}\right) \tag{5c}$$

$$F_D(u,v,\theta) = \mu\delta'\left(mf\cos\theta + u\sin\frac{\theta}{m} + v\cos\frac{\theta}{m}\right) * mf\cos\theta + u\sin\frac{\theta}{m} + v\cos\frac{\theta}{m} \tag{5d}$$

$$F_I(\theta) = -m^2\omega^2\mu f'\sin\theta \tag{5e}$$

and $\alpha_{n+2} = \epsilon\alpha'_{n+2}$, $\gamma = \epsilon\gamma'$, $\delta = \epsilon\delta'$, $f = \epsilon f'$.

Averaging of the transformed system [Equation (5)] results in the following ($N = 3$):

$$\begin{pmatrix}\dot{u}\\ \dot{v}\end{pmatrix} = -\frac{\epsilon}{2m\omega}\left[S(u,v)\begin{pmatrix}u\\ v\end{pmatrix} + \frac{1}{m\pi}\begin{pmatrix}I_S(u,v,\theta)\\ I_C(u,v,\theta)\end{pmatrix} + \delta_{m,1}\begin{pmatrix}-\omega^2\mu f'\\ 0\end{pmatrix}\right] \tag{6a}$$

where

$$S(u,v) = \begin{pmatrix} m\omega\gamma' & -\Omega + \frac{3}{4}m^2\alpha'_3(u^2+v^2)\\ \Omega - \frac{3}{4}m^2\alpha'_3(u^2+v^2) & m\omega\gamma'\end{pmatrix} \tag{6b}$$

$$\begin{pmatrix}I_S(u,v)\\ I_C(u,v)\end{pmatrix} = \begin{pmatrix}\int_0^{2m\pi} F_D(u,v,\theta)\sin\frac{\theta}{m}d\theta\\ \int_0^{2m\pi} F_D(u,v,\theta)\cos\frac{\theta}{m}d\theta\end{pmatrix} \tag{6c}$$

and $\delta_{m,1}$ is a Kronecker delta function ($\delta_{m,1} = 1$ for $m = 1$ and $\delta_{m,1} = 0$ for $m \neq 1$).

Note that the Kronecker delta function determines the existence of an averaged forcing term near primary resonance ($m = 1$). Consequently, subharmonic resonances ($m > 1$) are not excited by the averaged inertial forcing.

By employing a polar transformation [$J = 1/2(u^2+v^2)$, $\Phi = \tan^{-1}(v/u)$], the averaged system [Equation (6)] can be written as a perturbed Hamiltonian system: $d\mathbf{q}/dt = \mathbf{F}(\mathbf{q}) + \delta^*\mathbf{G}(\mathbf{q},\theta)$ where $\mathbf{q} = (J,\Phi)^T$. This system consists of an integrable potential function [$\mathbf{F} = (F_1(\mathbf{q}),F_2(\mathbf{q}))^T$] perturbed by a damping mechanism [$\mathbf{G} = (G_1(\mathbf{q},\theta), G_2(\mathbf{q},\theta))^T$], where there exists an invariant quantity ($H(\mathbf{q})$ such that $F_1(\mathbf{q}) = -\partial H(\mathbf{q})/\partial\Phi$ and $F_2(\mathbf{q}) = \partial H/\partial J$. The potential function consists of the averaged mooring restoring force excited near primary resonance by an averaged inertial force, whereas the damping perturbation includes the averaged drag force complemented by structural damping.

$$\begin{pmatrix} \dot{J} \\ \dot{\Phi} \end{pmatrix} = \begin{pmatrix} F_1(J,\Phi) \\ F_2(J,\Phi) \end{pmatrix} + \delta^* \begin{pmatrix} G_1(J,\Phi) \\ G_2(J,\Phi) \end{pmatrix} \tag{7a}$$

where

$$F_1(J,\Phi) = \delta_{m,1} f^* (2J)^{1/2} \cos\Phi \tag{7b}$$

$$F_2(J,\Phi) = -\Omega^* + \alpha_3^* (2J) - \delta_{m,1} f^* (2J)^{-1/2} \sin\Phi$$

$$G_1(J,\Phi) = -\gamma^*(2J) - (2J)^{1/2} [I_S(J,\Phi)\cos\Phi + I_C(J,\Phi)\sin\Phi] \tag{7c}$$

$$G_2(J,\Phi) = -(2J)^{-1/2} [I_C(J,\Phi)\cos\Phi - I_S(J,\Phi)\sin\Phi]$$

$$\begin{pmatrix} I_S(J,\Phi) \\ I_C(J,\Phi) \end{pmatrix} = \begin{pmatrix} \int_0^{2m\pi} D(J,\Phi,\theta)|D(J,\Phi,\theta)|\sin\frac{\theta}{m}\mathrm{d}\theta \\ \int_0^{2m\pi} D(J,\Phi,\theta)|D(J,\Phi,\theta)|\cos\frac{\theta}{m}\mathrm{d}\theta \end{pmatrix} \tag{7d}$$

$$D(J,\Phi,\theta) = f\cos\theta - \sqrt{2J}\sin\left(\frac{\theta}{m} + \Phi\right) \tag{7e}$$

and

$$\delta^* = \frac{\mu\delta}{\pi\omega}$$

$$\Omega^* = \frac{\omega^2 - m^2\alpha_1}{2m\omega} \qquad \alpha_3^* = \frac{m\alpha_3}{\omega}$$

$$\gamma^* = \frac{\pi\omega\gamma}{2\mu\delta} \qquad f^* = \frac{1}{2}\mu\omega f.$$

The Hamiltonian energy can be found by integrating the averaged system [Equation (7), $\delta^* = 0$]

$$H(J,\Phi) = -\Omega^* J + \alpha_3^* J^2 - \delta_{m,1} f^* \sqrt{2J}\sin\Phi. \tag{8}$$

The structure of the Hamiltonian system (Fig. 2) is described by the characteristics of its fixed points [$\mathrm{d}\mathbf{q}/\mathrm{d}t = 0 : (J,\Phi)_e$] which are the roots of the following equation [$z_i = (2J)_i$, $i = 1,2,3$]:

$$z^3 - 2\left(\frac{\Omega^*}{\alpha_3^*}\right) z^2 + \left(\frac{\Omega^*}{\alpha_3^*}\right)^2 z - \delta_{m,1}\left(\frac{f^*}{\alpha_3^*}\right)^2 = 0. \tag{9}$$

The structure of near resonance subharmonic response ($m > 1$) is always characterized by a unique center [$(J,\Phi)_e = (1/2\Omega^*/\alpha_3^*,\phi)$], whereas the structure of the solution near primary resonance ($m = 1$) consists of either unique centers [$(J,\Phi)_e = (j_1,\phi_1)$] or of two coexisting centers [$(J,\Phi)_e = (j_1,\pi/2)$ and $(j_3,3\pi/2)$] separated by a hyperbolic saddle [$(J,\Phi)_e = (j_2, 3\pi/2)$]. The primary resonance structure defines a classical jump bifurcation set where existence of unique ($f > \beta_c^H$) or coexisting centers ($f < \beta_c^H$) is defined in parameter space by the following bifurcation value:

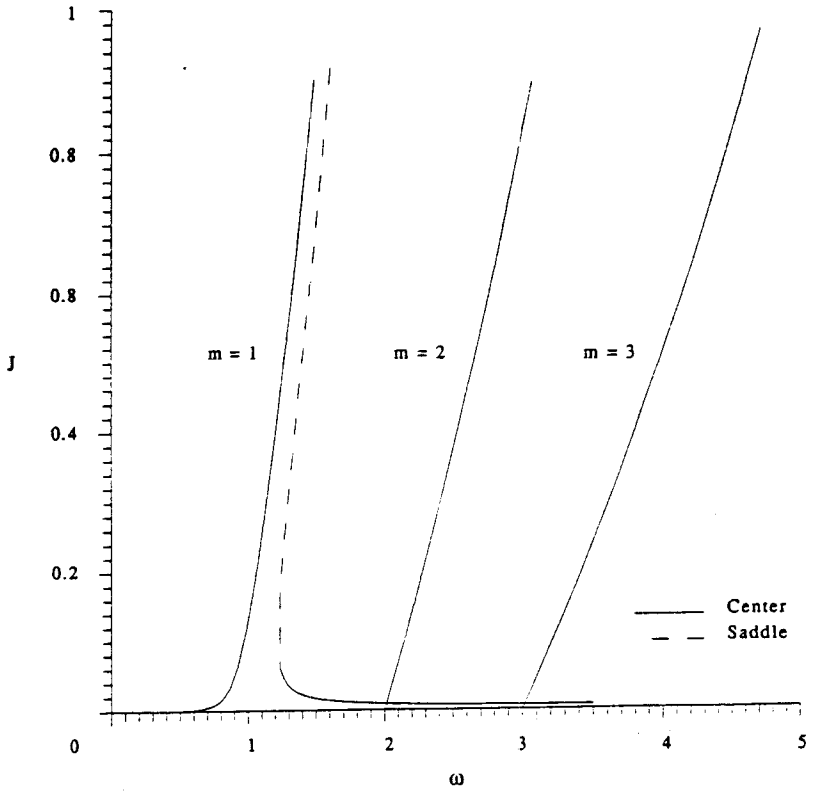

FIG. 2. Structure of the averaged Hamiltonian system.

$$\beta_c^H = \left(\frac{2}{3}\right)^2 \frac{(\omega^2 - \alpha_1)^{3/2}}{\mu\,\omega^2\sqrt{\alpha_3}}. \tag{10}$$

Note that for the linearized mooring system ($\alpha_3 = 0$) there exists a unique center $[(J, \Phi)_e = (1/2(f^*/\Omega^*)^2, \pi/2)]$, which is identical to the anticipated response of a linear harmonically excited, undamped oscillator.

3.2. *Primary resonance*

Stability of the averaged system near primary resonance ($m = 1$) is performed analytically by characterization of the system's fixed points where the damping perturbation ($\mathbf{G}(J,\Phi)$: Equation (7c)) can be written out explicitly:

$$\begin{pmatrix} \dot{J} \\ \dot{\Phi} \end{pmatrix} = \begin{pmatrix} F_1(J,\Phi) \\ F_2(J,\Phi) \end{pmatrix} + \delta^* \begin{pmatrix} G_1(J,\Phi) \\ G_2(J,\Phi) \end{pmatrix} \tag{11a}$$

where

$$F_1(J,\Phi) = f^*\,(2J)^{1/2}\cos\Phi$$

$$F_2(J,\Phi) = -\Omega^* + \alpha_3^*\,(2J) - f^*\,(2J)^{-1/2}\sin\Phi \tag{11b}$$

$$G_1(J,\Phi) = -\gamma^*(2J) - \frac{4}{3}\sqrt{f^2 + 2f\sqrt{2J}\sin\Phi + (2J)}\,[(2J) + f\sqrt{2J}\sin\Phi]$$

$$G_2(J,\Phi) = -\frac{4}{3}\sqrt{f^2 + 2f\sqrt{2J}\sin\Phi + (2J)}\left(\frac{f\cos\Phi}{\sqrt{2J}}\right). \tag{11c}$$

Thus, the fixed points are the roots $[z_i = (2J)_i, \Phi_i]$ of the following coupled set of equations: $\mathbf{F}(J,\Phi) + \delta^*\mathbf{G}(J,\Phi) = 0$. Stability of the fixed points is characterized by solution of a standard eigenfunction: $\lambda^2 - p_i\lambda + q_i = 0$, where p_i and q_i are the trace and determinant of the derivative matrix (evaluated for each fixed point i), respectively. Asymptotic stability is defined by negative real parts of the derivative matrix. For small values of δ^* we assume a perturbed solution form to [Equation (11)]:

$$\begin{aligned} J_i &= j_i + \epsilon_i \\ \Phi_i &= \phi_i + \eta_i \end{aligned} \tag{12}$$

where $(j,\phi)_i$ are solutions to the Hamiltonian system ($\delta^* = 0$) and $(\epsilon,\eta)_i$ are $o(\delta^*)$.

Stability of the perturbed fixed points is then obtained by evaluation of the eigenfunction coefficients to $O(\delta^*)$:

$$p_i = -\gamma - 4\delta^*\sqrt{\Gamma_i(J,\Phi)}$$

$$q_i = [\Omega^* - \alpha_3^*(2J_i)][\Omega^* - 3\alpha_3^*(2J_i)] + \frac{8}{3}\delta^* f\sqrt{\frac{\Gamma_i(J,\Phi)}{2J_i}}\left\{\Omega^* - \alpha_3^* f(2J)_i\frac{f + \sqrt{2J_i}\sin\Phi}{\Gamma_i(J,\Phi)}\right\}\cos\Phi_i \tag{13}$$

where

$$\Gamma_i(J,\Phi) = f^2 + 2f\sqrt{2J_i}\sin\Phi_i + (2J_i).$$

Substitution of Equation (12) into the coupled set of equations and their expansion in a Taylor series for functions of two variables results in the following values of $(\epsilon,\eta)_i$ to $O(\delta^*)$:

$$\begin{aligned} \epsilon_i &= 0 \\ \eta_i &= \left(\frac{4\delta^*}{3f^*}\right)\left[(f \pm \sqrt{2j_i})^2 \pm \left(\frac{3}{4}\right)\gamma^*\sqrt{2j_i}\right] \end{aligned} \tag{14}$$

where the upper choice of sign refers to $i = 1$ and the lower choice of sign refers to $i = 2,3$.

But as $\sin\Phi \to \pm 1$, $-\cos\Phi \to \pm\eta$ and as η is of $O(\delta^*)$, stability of the system fixed points is found to be governed by the following coefficients:

$$p_i = -\gamma - 4\delta^*(f \pm \sqrt{2j_i})$$

$$q_i = [\Omega^* - \alpha_3^*(2j_i)][\Omega^* - 3\alpha_3^*(2j_i)]. \tag{15}$$

Consequently, $(J,\Phi)_1$ and $(J,\Phi)_3$ are the hyperbolic sinks ($q_{1,3} > 0$) and $(J,\Phi)_2$ remains a hyberbolic saddle ($q_2 < 0$). While $(J,\Phi)_1$ is always an attractor ($p_1 < 0$), $(J,\Phi)_3$ exists only in limited parameter space ($f < \beta_c^P$) defined by the following bifurcation value:

$$\beta_c^P = \frac{2}{3}\sqrt{\frac{\omega^2 - \alpha_1}{\alpha_3}} - \frac{\pi}{4}\frac{\omega}{\mu}\frac{\gamma}{\delta}. \tag{16}$$

Furthermore, coexistence of attractors $(J,\Phi)_{1,3}$ will only occur for stable values of $(J,\Phi)_3$ [$p_3 < 0$: $(f + 1/2\gamma^*)^2 < (2j_3) < (\Omega^*/3\alpha_3^*)$] and is controllable by the magnitude of the relative damping, γ^* (Fig. 3). This result is verified by numerical simulation of the system [Equation (2)] itself resulting in two coexisting attractors (Fig. 4). Thus, stability analysis of the Poincaré map, portrayed by the perturbed averaged system near primary resonance, ensures global attraction for larger excitation values and describes conditions for coexistence of solutions in the system.

3.3. *Subharmonic resonance*

Stability of the averaged system near subharmonic resonance ($m > 1$) can be performed by numerically characterizing the system's fixed points. In order to obtain approximate analytical stability criteria, upper and lower bounds of the nonlinear

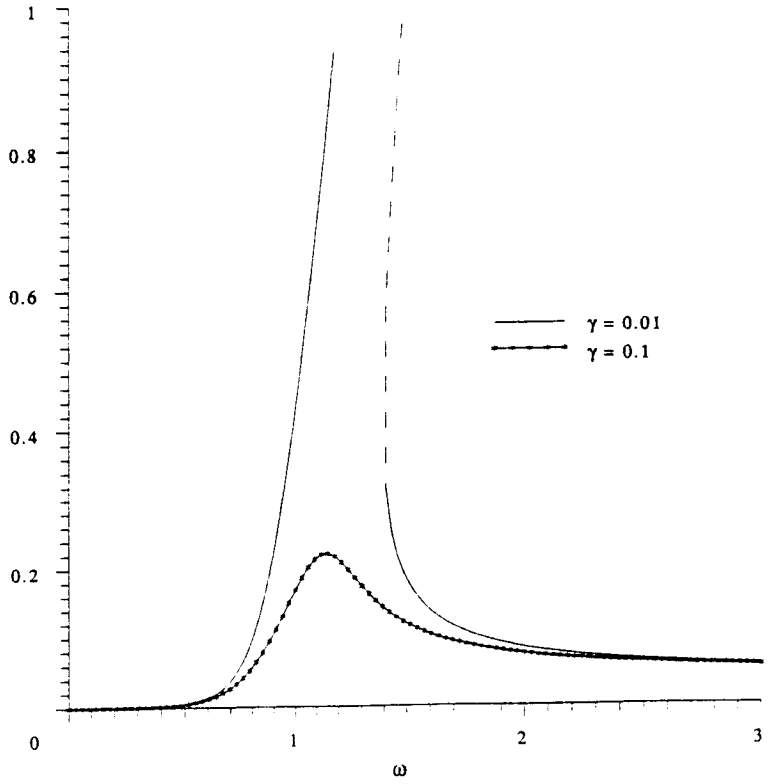

FIG. 3. Primary resonant structure of averaged system.

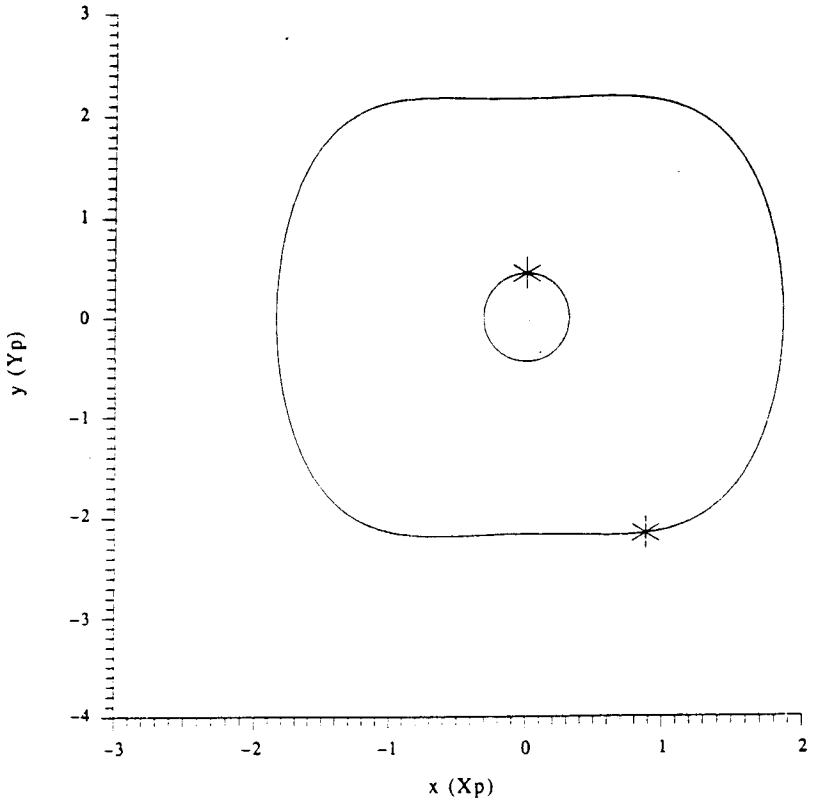

FIG. 4. Coexisting attractors (m = 1): phase plane and Poincaré map.

viscous drag component are evaluated. By substitution of the relative motion term [$D(J,\Phi,\theta)$: Equation (7e)] with its upper ($|\sqrt{(2J)}\sin(\theta/m+\Phi|$) and lower ($|mf\cos\theta|$) values, the drag integrals [$I_{S,C}(J,\Phi)$: Equation (7d)] are calculated and limiting values for the damping perturbation [$\mathbf{G}(J,\Phi)$: Equation (7c)] are formulated explicitly. The upper ($\mathbf{G}^U$) and lower bounds ($\mathbf{G}^L$) of the damping perturbation correspond to assumptions on the relative magnitude of the ocean system response.

$$\begin{pmatrix}\dot{J}\\ \dot{\Phi}\end{pmatrix} = \begin{pmatrix}F_1(J,\Phi)\\ F_2(J,\Phi)\end{pmatrix} + \delta^*\begin{pmatrix}G_1^{L,U}(J,\Phi)\\ G_2^{L,U}(J,\Phi)\end{pmatrix} \tag{17a}$$

where

$$F_1(J,\Phi) = 0 \tag{17b}$$

$$F_2(J,\Phi) = -\Omega^* + \alpha_3^*(2J)$$

$$G_1^L(J,\Phi) = -(\gamma^* + f)(2J) \tag{17c}$$

$$G_2^L(J,\Phi) = 0$$

or

$$G_1^U(J,\Phi) = -\gamma^*(2J) - \left(\frac{4}{3m}\right)(2J)^{3/2} + \delta_{m,(2n+1)}\left(\frac{4}{m(m^2-4)}\right) f(2J)\sin m\Phi \tag{17d}$$

$$G_2^U(J,\Phi) = \delta_{m,(2n+1)}\left(\frac{2}{m^2-4}\right) f\cos m\Phi$$

and $\delta_{m,(2n+1)}$ is a Kronecker delta function ($\delta_{m,(2n+1)} = 1\ \forall m = 2n+1$; $\delta_{m,(2n+1)} = 0\ \forall m \neq 2n+1$), where n denotes the index of an odd series ($n = 1,3,5, \ldots, N$).

Note that the Kronecker delta function determines the existence of additional damping components for odd subharmonics ($m = 2n+1$, $n = 1,3, \ldots, N$) in $\mathbf{G}^U$ [Equation (17d)].

The lower bound ($\mathbf{G}^L$) is valid for small amplitude motions ($\sqrt{2J} \ll mf$) and is representative of drag equivalent linearization techniques [$F_D \propto (U - dx/dt)|U|$ in Equation (1c)] whereas the upper bound ($\mathbf{G}^U$) is valid for large motions ($\sqrt{2J} \gg mf$) corresponding to near resonant response [$F_D \propto (U - dx/dt)|dx/dt|$] which is consistent with the averaging theorem and was previously identified by the detuning parameter ($\epsilon\Omega = \omega^2 - m^2\alpha_1$).

The fixed points of near resonant averaged subharmonic system [Equation (17)] are the roots [$z_i = (2J)_i$; $i = 1,2,3,4$] of the following equation:

$$z^2 + \left[\left(\frac{2}{3}\frac{\delta^*}{\alpha_3^*}\right)^2 - 2\left(\frac{\Omega^*}{\alpha_3^*}\right)\right] z + \left(\frac{m\gamma\delta^*}{3(\alpha_3^*)^2}\right)\sqrt{z} + \left[\left(\frac{\Omega^*}{\alpha_3^*}\right)^2 + \left(\frac{m}{4}\right)^2\left(\frac{\gamma}{\alpha_3^*}\right)^2 - \delta_{m,(2n+1)}\left(\frac{2f\delta^*}{(m^2-4)\alpha_3^*}\right)^2\right] = 0. \tag{18}$$

Stability of the fixed points is characterized by the following coefficients evaluated for each fixed point i, respectively:

$$p_i = -\left(\frac{m}{2}\right)^2\gamma - \frac{2}{3}\frac{m^2+2}{m}\delta^*\sqrt{2J_i}$$

$$q_i = (2\alpha_3^*)^2(2J_i)^2 + \left[2\left(\frac{2}{3}\delta^*\right)^2 - 4\Omega^*\alpha_3^*\right](2J_i) + \frac{m}{3}\gamma\delta^*\sqrt{2J_i}. \tag{19}$$

The structure of the averaged subharmonic system for very small values of structural damping ($\gamma \ll \delta < 1$) can be described (Fig. 5) by a saddle-node bifurcation as there exist to $O(\delta^*)$ four possible roots to [Equation (18)] for the following bifurcation value ($f > \beta_c^S$):

$$\beta_c^S = \frac{m^2-4}{3}\sqrt{\frac{\Omega^*}{\alpha_3^*} - \left(\frac{\delta^*}{3\alpha_3^*}\right)^2}. \tag{20}$$

Therefore, the fixed points [$(J,\Phi)_i$, $i = 1, \ldots, 4$] are hyperbolic saddles ($q_{1,3} < 0$) and attractors ($p_{2,4} < 0$, $q_{2,4} > 0$). Furthermore, the linearized system ($\alpha_{n>1} = 0$) reveals

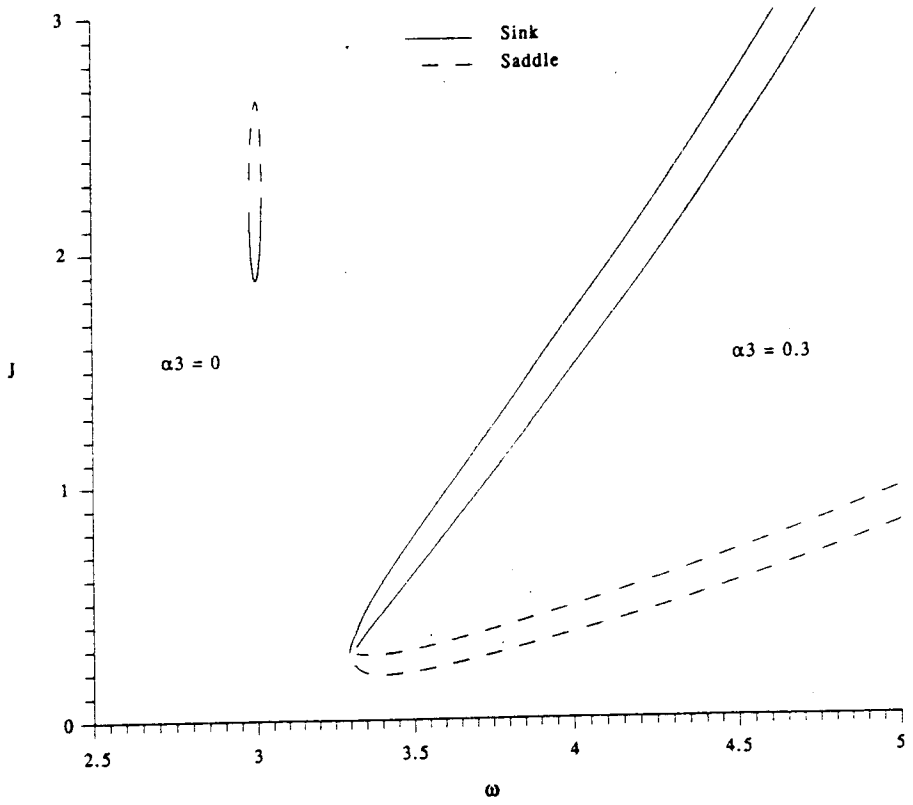

FIG. 5. Subharmonic structure ($m = 3$) of averaged system.

existence of two roots ($f > \beta_c^S$), which are a stable attractor ($p_1 < 0$, $q_1 > 0$) and a saddle ($q_2 < 0$)

$$\beta_c^S = \frac{m^2-4}{2}\frac{\Omega^*}{\delta^*}. \tag{21}$$

Note the narrow domain of existence for the subharmonic solution of the linearized system vs that with the nonlinear restoring force (Fig. 5). Numerical simulation of the system [Equation (2)] verifies the existence of subharmonic response for the values predicted above (Fig. 6). Thus, stability analysis of the Poincaré map defines coexistence of solutions near subharmonic resonance.

4. EXISTENCE OF PERIOD DOUBLING

In order to investigate the stability of solutions which are not necessarily near resonance, a local variational approach is employed. This consists of perturbing an approximate system solution and evaluating its stability by analyzing the general Hill's system obtained from linearization of the corresponding variational. The results identify two domains of stability loss of the mT periodic solution. The first corresponds to the

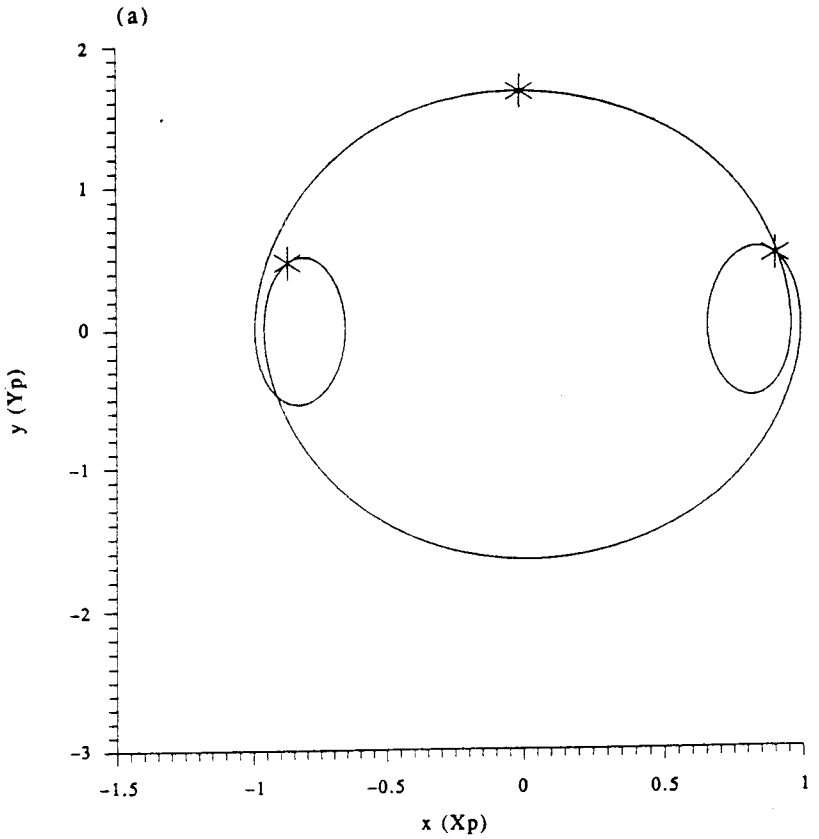

FIG. 6. Subharmonic solution ($3T$): (a) phase plane and Poincaré map, (b) power spectra.

resonant tangent bifurcations which were found by generalized averaging in Section 3 and the second consists of a period doubling bifurcation.

4.1. *Periodic solutions*

An approximate system solution can be obtained by a variety of methods (e.g. Nayfeh and Mook, 1979) but the method of harmonic balance (Hayashi, 1964) is chosen in order to account for the even harmonics induced by the bias created by the nonlinear viscous drag

$$x_0 \cong A_0 + \sum_i A_{i/m} \cos\left(i\frac{\theta}{m} + \Psi_{i/m}\right)$$

$$y_0 \cong -\frac{\omega}{m}\sum_i iA_{i/m} \sin\left(i\frac{\theta}{m} + \Psi_{i/m}\right) \tag{22}$$

where A_0, $A_{i/m}$, $\Psi_{i/m}$ are solution amplitudes and phases, I is the order of approximation ($i = 1,2,3, \ldots, I$) and m is the order of subharmonic.

The unknown amplitudes and phases are obtained by substitution of the approximate

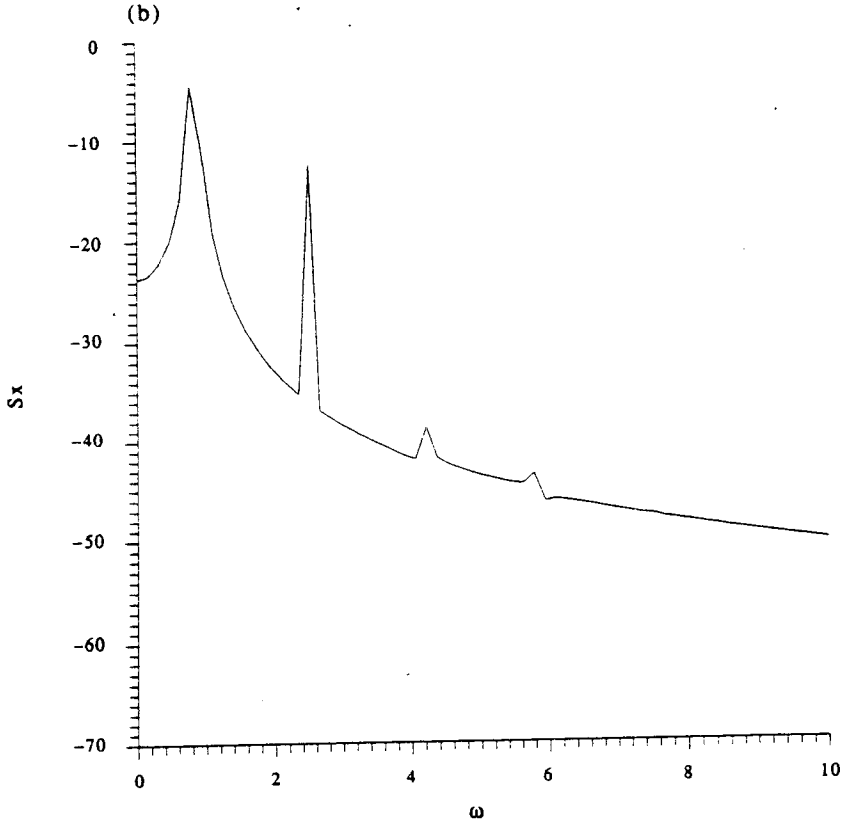

FIG. 6. (Continued).

solution [Equation (22)] into the system [Equation (2)], squaring the resultant equation and comparing terms of equal harmonic order. Thus, the system is transferred into a finite nonlinear set of algebraic equations:

$$S_j(A_0, A_{i/m}, \Psi_{i/m}) = 0 \tag{23}$$

where $j = 1,2,3, \ldots, 2I+1$ [see Appendix A1 for detail: S_j; $j = 1,2,3$].

Solution of the set with an iterative Newton–Raphson procedure results in a frequency response relationship (ω-A_m) (Fig. 7). An unsymmetric solution includes even and odd harmonics [$x_0(t)$, $y_0(t) \neq x_0(t+mT/2)$, $y_0(t+mT/2)$; $T = 2\pi/\omega$], whereas a symmetric solution consists of only odd harmonics.

A low order solution ($I = 1$) for a linearized mooring system ($\alpha_{n>1} = 0$) or for a weakly nonlinear small angle mooring configuration, yields the anticipated amplitudes and phase of a biased linear oscillator:

$$A_0 = \sqrt{\frac{3}{8}\frac{\mu\delta}{\alpha_1}}\,(f^2 + 2fA_1\sin\Psi_1 + A_1^2)$$

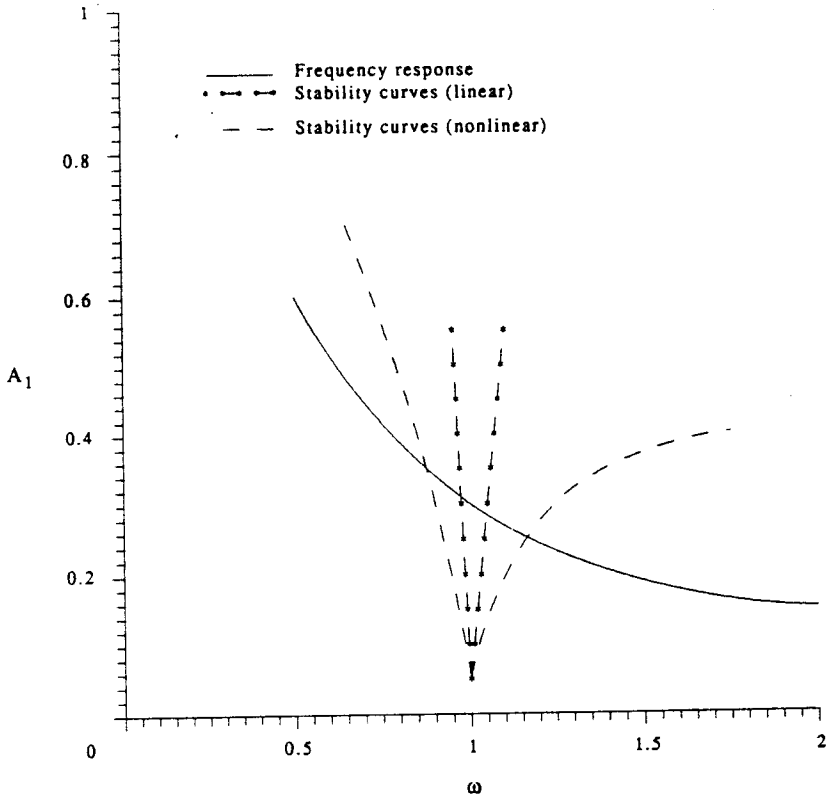

FIG. 7. Stability diagram of T periodic solution.

$$A_1 = \frac{\mu\,\omega^2 f}{\sqrt{(\alpha_1-\omega^2)^2 + (\gamma\omega)^2}} \tag{24}$$

$$\Psi_1 = \tan^{-1}\left(-\frac{\alpha_1-\omega^2}{\gamma\,\omega}\right).$$

Note that the bias is identified by the drag parameter even to this order.

4.2. *Variational system*

Local stability is determined by considering a perturbed solution $(x(t), y(t))$ where $(x_0(t), y_0(t))$ is an approximate solution and $(\epsilon(t), \eta(t))$ is a small variation

$$x(t) = x_0(t) + \epsilon(t) \tag{25}$$

$$y(t) = y_0(t) + \eta(t).$$

Substituting the solution $(x(t), y(t))$ in the equation of motion [Equation (2)] and simplifying the resulting equation, leads to the following nonlinear variational system:

$$\dot{\epsilon} = \eta \tag{26a}$$

$$\ddot{\eta} = P(\eta,\theta) + Q(\epsilon,\theta)$$

where

$$P(\eta,\theta) = -\gamma\eta + \mu\delta\left(f\cos\theta - \frac{y_0(\theta)+\eta}{\omega}\right)\left|f\cos\theta - \frac{y_0(\theta)+\eta}{\omega}\right| - \mu\delta\left(f\cos\theta - \frac{y_0(\theta)}{\omega}\right)\left|f\cos\theta - \frac{y_0(\theta)}{\omega}\right| \tag{26b}$$

$$Q(\epsilon,\theta) = -\sum_n \alpha_n\{[x_0(\theta) + \epsilon]^n - x_0^n(\theta)\}. \tag{26c}$$

Linearizing the variational [Equation (26)] yields a linear ordinary differential equation with periodic coefficient functions $H_{1,2}[x_0(t), y_0(t)] = H_{1,2}[x_0(t+mT), y_0(t+mT)]$.

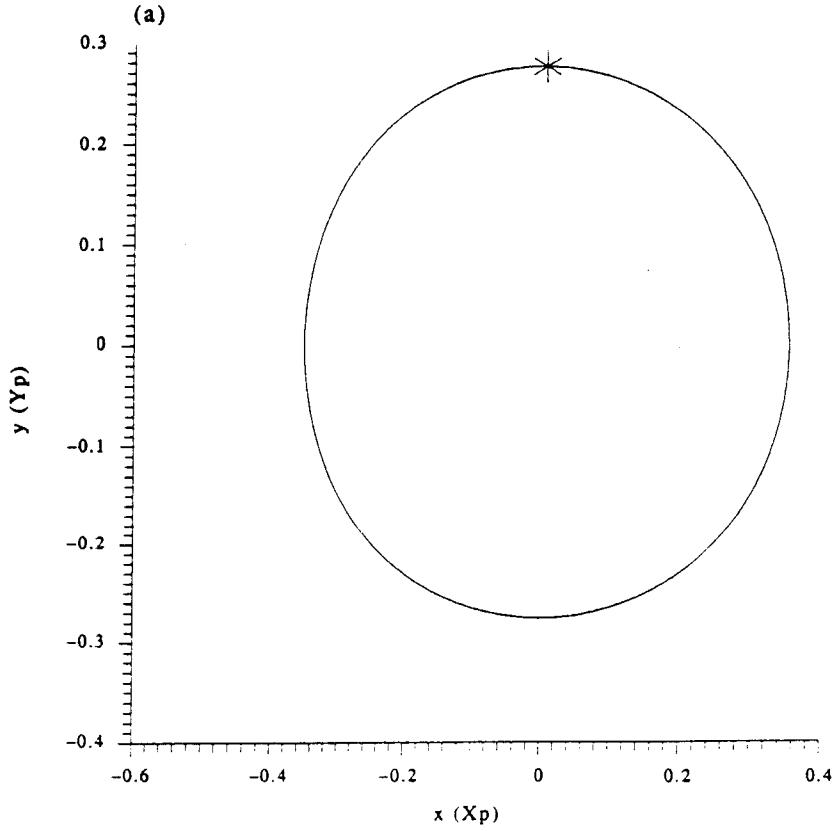

FIG. 8. Loss of stability and period doubling: (a) phase plane and Poincaré map, (b) power spectra. [(1) T, (2) $2T$.]

(26a)

(26b)

(26c)

it l equation
)($+mT$)].

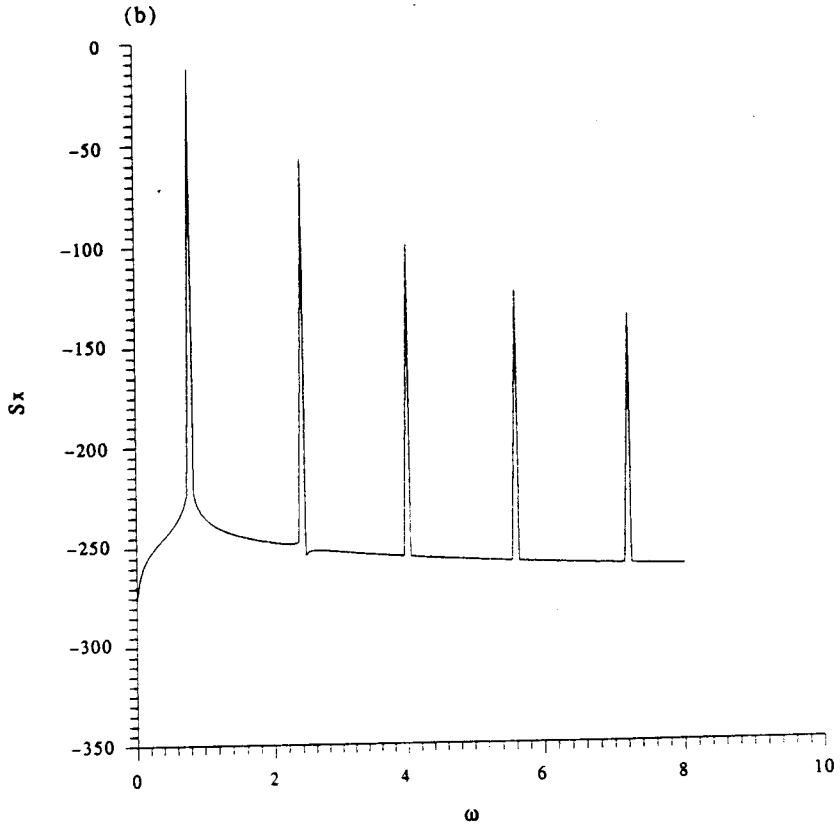

FIG. 8. (Continued).

$$\dot{\epsilon} = \eta \tag{27a}$$
$$\dot{\eta} = H_1(y_0)\,\eta + H_2(x_0)\,\epsilon$$

where

$$H_1 = -\gamma - 2\frac{\mu\delta}{\omega}\left|f\cos\theta - \frac{y_0(\theta)}{\omega}\right| \tag{27b}$$

$$H_2 = -\sum_n n\,\alpha_n\,x_0^{n-1}(\theta). \tag{27c}$$

Substituting the approximate T periodic solution [$m = 1$, Equation (22)] in Equation (27) and expanding $H_{1,2}(x_0,y_0)$ in Fourier series [$H_{1,2}(\theta)$] leads to a general Hill's variational system:

)).4

$$\dot{\epsilon} = \eta \tag{28a}$$
$$\dot{\eta} = H_1(\theta)\eta + H_2(\theta)\,\epsilon$$

ov r spectra. [(1)

where

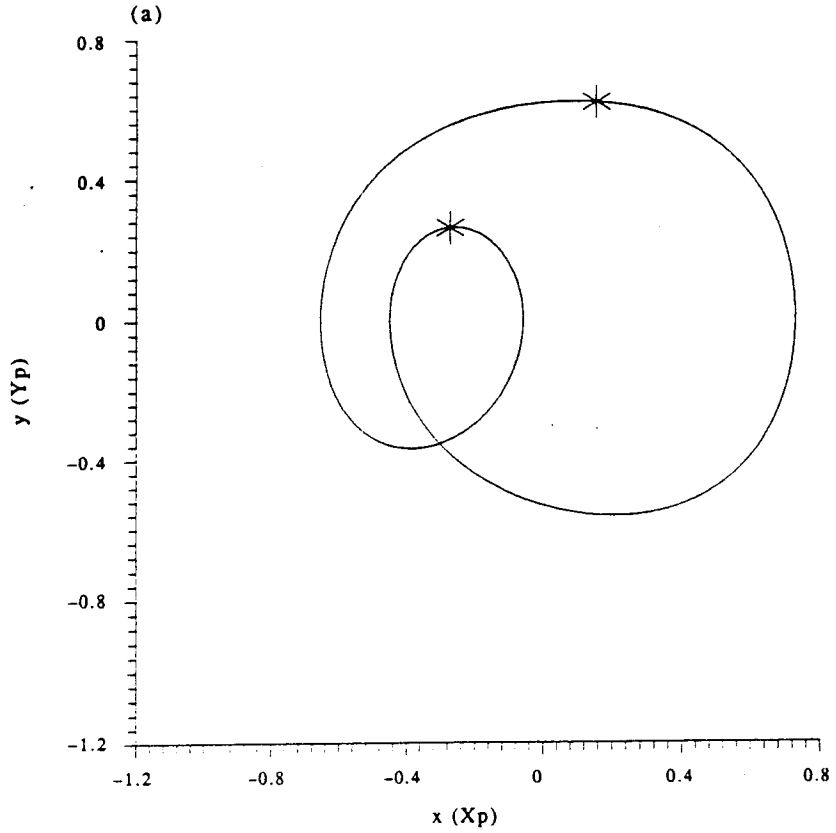

FIG. 8. (Continued).

$$H_1(\theta) = -\gamma - 2\frac{\mu\,\delta}{\omega}\,|\xi_{C1}\cos\theta + \xi_{S1}\sin\theta| \tag{28b}$$

$$H_2(\theta) = \zeta_0 + \sum_j \zeta_{Cj}\cos j\theta + \zeta_{Sj}\sin j\theta \tag{28c}$$

and $\xi_j = \xi_j(A_0,A_i,\Psi_i)$, $\zeta_j = \zeta_j(A_0,A_i,\Psi_i)$; $j = 1,2,3, \ldots, J$ [see Appendix A2 for $(\xi, \zeta)_j$].

4.3. *Stability and period doubling*

The particular solution to Equation (28) is $\epsilon = \exp(\nu t)Z(t)$. Application of Floquet theory (Ioos and Joseph, 1981) yields two solution forms: $Z(t) = Z(t+T)$, $Z(t) = Z(t+2T)$, which are due to the odd and even terms in Equation (22), respectively. Thus, two unstable regions are defined. The first unstable region, corresponding to $Z(t) = Z(t+T)$, is identified by the even terms ($m = 1 : j = 2,4,6, \ldots$) in Equation (28) and coincides with the vertical tangent points of a primary resonance on the frequency response curve. The second unstable region, corresponding to $Z(t) = Z(t+2T)$, is identified by the odd terms ($m = 1 : j = 1,3,5, \ldots$) and reveals a secondary resonance which consists of a period doubled solution.

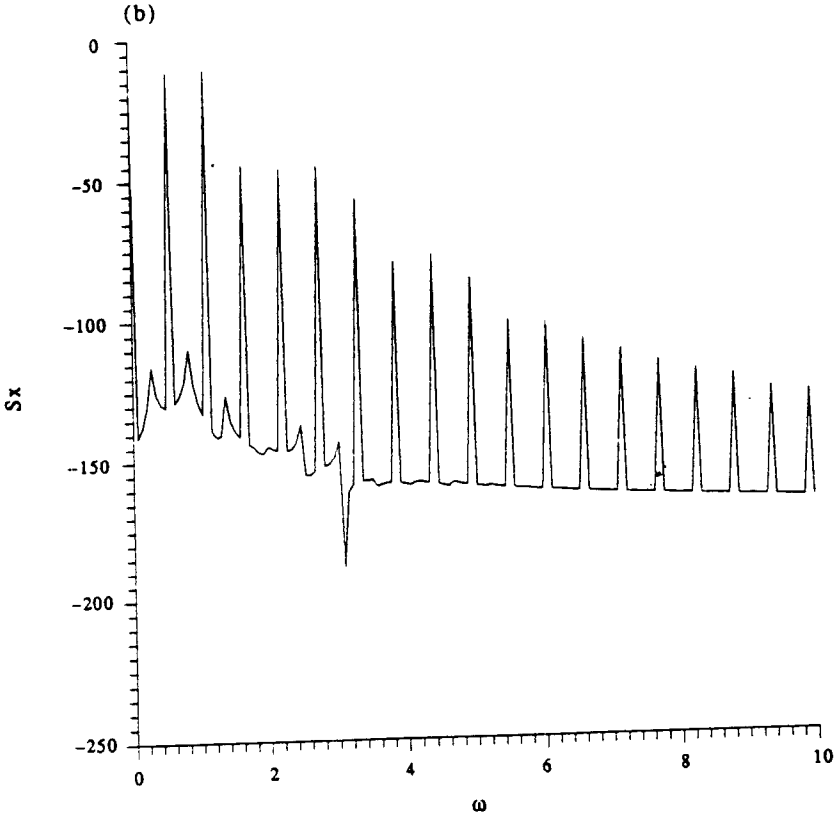

FIG. 8. (Continued).

The boundaries of the unstable regions can be obtained by applying the method of harmonic balance to Hill's equation [Equation (28)] for $\epsilon(t)$ at the stability limit ($\nu = 0$)

$$\epsilon(\theta) = b_0 + \sum_j b_j \cos(j\theta + \Psi_j) \quad ; \quad Z(t+T) \tag{29a}$$

$$\epsilon(\theta) = \sum_j b_j \cos\left(\frac{j}{2}\theta + \Psi_{j/2}\right) \quad ; \quad Z(t+2T). \tag{29b}$$

The condition for a non-zero solution results in a determinant [$\Delta(\omega^2) = 0$] from which two hyperbolic stability curves defining the unstable primary and secondary resonance regions [$\Delta(\omega^2) < 0$ for $\nu > 0$] are obtained. Intersection of approximate stability curves with the frequency response curve define in parameter space the domain of stability loss of the T periodic solution. The first stability region is obtained by the first solution form [Equation (28a)] and corresponds to the primary resonance. The second stability region is obtained by the period doubled solution form [Equation (28b)] and defines the secondary subharmonic resonance (Fig. 7)

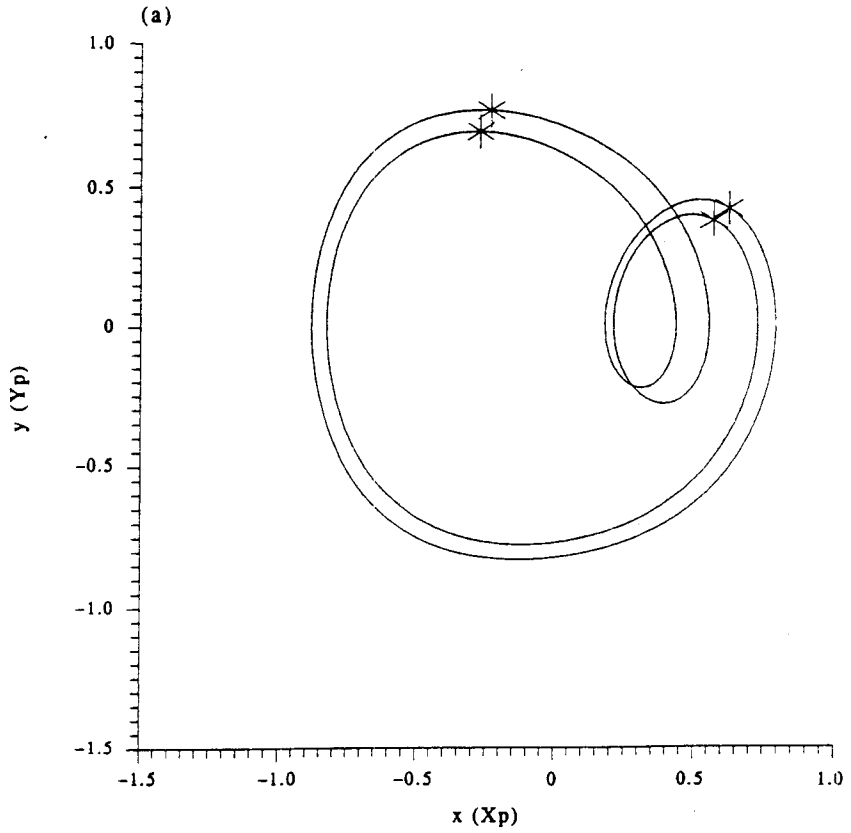

FIG. 9. Evolution of an attractor via period doubling bifurcations: (a) phase plane and Poincaré map, (b) power spectra. [(1) $4T$, (2) chaos.]

$$\Delta(\omega^2) = \left[\zeta_0 - \left(\frac{\omega}{2}\right)^2\right]^2 - \frac{1}{4}(\zeta_{C1}^2 + \zeta_{S1}^2) + \left(\frac{\gamma\omega}{2}\right)^2 + sgn(\sigma)\frac{\mu\delta}{2}(\xi_{C1}\zeta_{S1} + \xi_{S1}\zeta_{C1}) - \left(\frac{\mu\delta}{2}\right)^2(\xi_{C1}^2 + \xi_{S1}^2) \tag{30}$$

where $\sigma = \xi_{C1}\cos\Psi_1 + \xi_{S1}\sin\Psi_1$ and $sgn\ (\sigma)$ denotes the sign of σ.

Numerical simulation of system [Equation (2)] response at the stability limit reveals the transition from a T periodic solution to a period doubled one depicted by the appearance of a strong bias and even harmonics both in the phase plane and power spectra (Fig. 8).

The stability criterion can be simplified for a weakly nonlinear small angle mooring configuration or for the linearized mooring system ($\alpha_{n>1} = 0$: $\zeta_0 = \alpha_1$, $\zeta_{C1} = \zeta_{S1} = 0$) resulting in a narrower unstable region (Fig. 7: linearized restoring force)

$$\Delta(\omega^2) = \left[\alpha_1 - \left(\frac{\omega}{2}\right)^2\right]^2 + \left(\frac{\gamma\omega}{2}\right)^2 - \left(\frac{\mu\delta}{2}\right)^2(f^2 + 2fA_1\sin\Psi_1 + A_1^2). \tag{31}$$

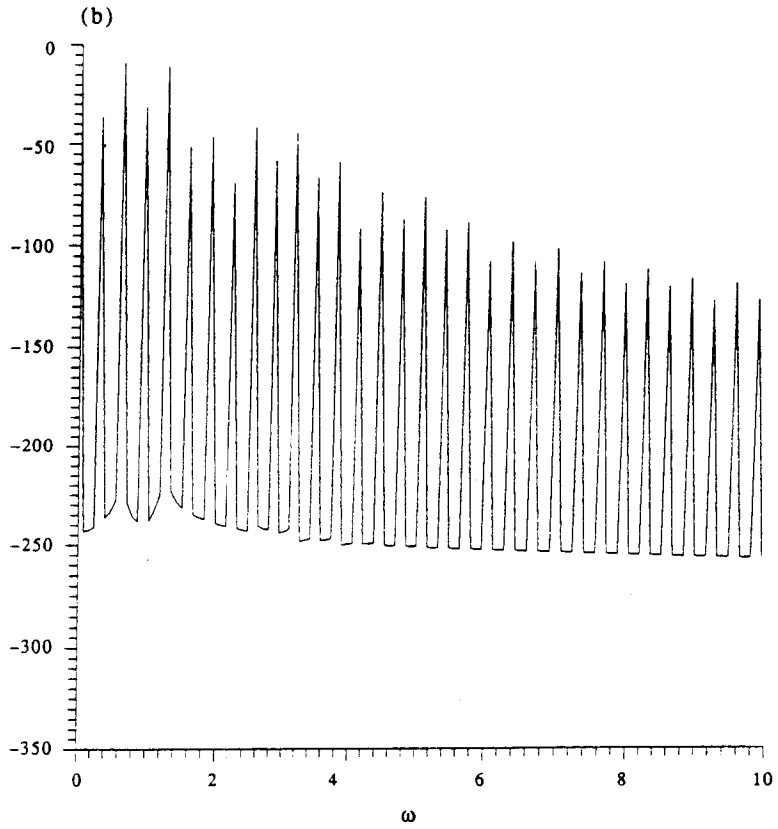

FIG. 9. (Continued).

Thus, the unstable region defining the secondary resonance can be shown to be confined between two hyperbolic functions [$\Delta(\omega) = 0$, $\gamma \ll \delta$) and is found to be sensitive to the magnitude of the response as indicated by:

$$A_1 \propto f + \left| \frac{4\alpha_1 - \omega^2}{2\mu\delta} \right|. \tag{32}$$

Note that the stability region of the undamped system [$\gamma,\delta=0$ in Equation (30)] is defined by the following criterion: $\omega^2 = 4\zeta_0 - 2\sqrt{(\zeta_{C1}^2 + \zeta_{S1}^2)}$, which is identical (to first order) to the secondary resonance stability region of the Duffing equation (Szemplinsk-Stupnika, 1987).

5. BIFURCATIONS AND ROUTES TO CHAOS

The subharmonic stability equation [Equation (17)] and the variational equation [Equation (27)] reveal regions where the mT periodic solution loses its stability. The transition to and from these steady states is defined by saddle-node (tangent) and period doubling (flip) bifurcations. These bifurcations are local and occur at the boundaries of the stability regions defined by Equations (20) and (30), respectively.

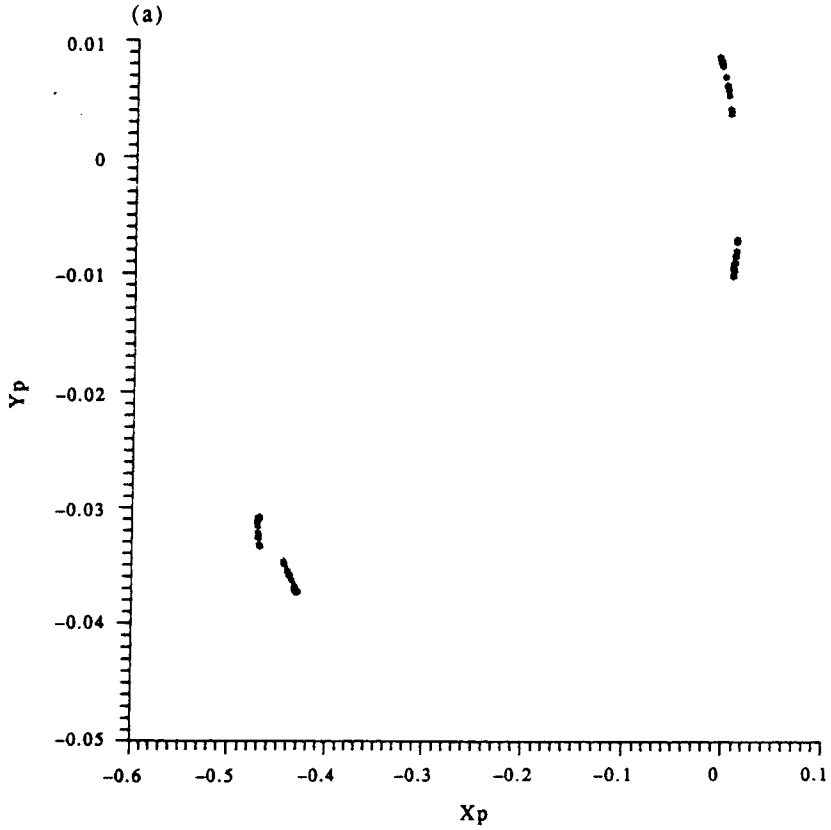

FIG. 9. (Continued).

Numerical integration of the system near the stability boundaries reveals the existence of continuing bifurcations and chaotic solutions. The numerical results are portrayed by phase plane diagrams (x,y), Poincaré maps $[Xp,Yp]$ where the mT subharmonic is depicted by a finite number of m points and the power spectra $[S_x(\omega)]$ where the order of the subharmonic is that of the peak with the largest energy content.

5.1. *Period doubling cascade*

In order to investigate stability of the $2T$ subharmonic, the solution $[M = 2; I = 2$ in Equation (22)] is substituted in the variational equation [Equation (27)] to obtain a subharmonic Hill's equation:

$$\dot{\epsilon} = \eta \tag{32a}$$

$$\dot{\eta} = H_1(\theta)\,\eta + H_2(\theta)\,\epsilon$$

where

$$H_1(\theta) = -\gamma - 2\frac{\mu\delta}{\omega}\left|\sum_{j=1}^{2}\xi'_{jC/2}\cos j\frac{\theta}{2} + \xi'_{jS/2}\sin j\frac{\theta}{2}\right| \tag{32b}$$

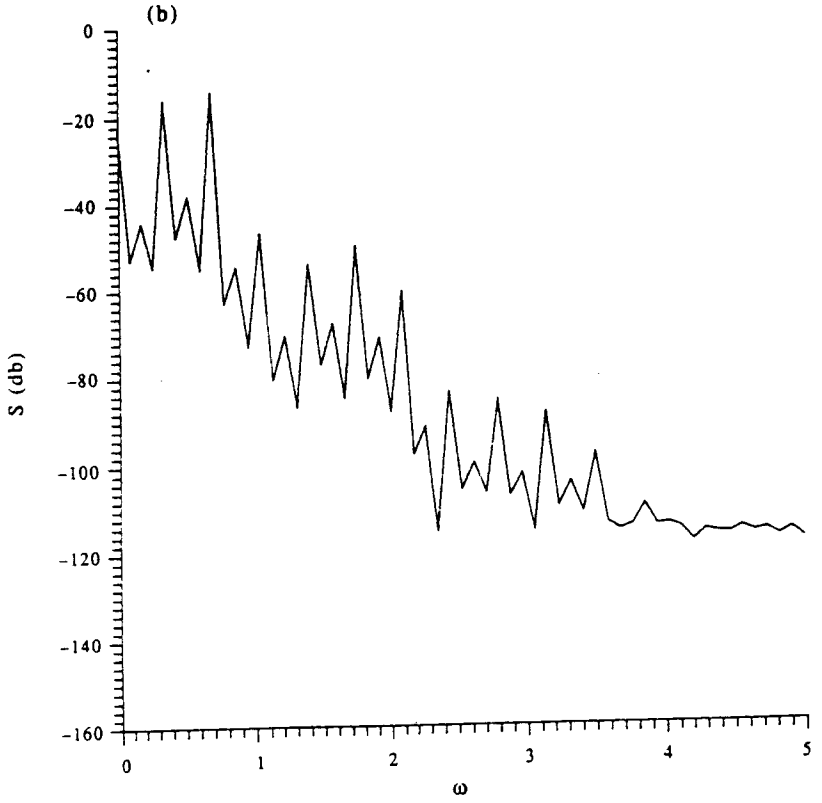

FIG. 9. (Continued).

$$H_2(\theta) = \zeta_0' + \sum_j \zeta_{jC/2}' \cos j\frac{\theta}{2} + \zeta_{jS/2}' \sin j\frac{\theta}{2} \tag{32c}$$

and $\xi_{j/2}' = \xi_{j/2}'(A_0, A_i, \Psi_i)$, $\zeta_{j/2}' = \zeta_{j/2}'(A_0, A_i, \Psi_i)$; $j = 1,2,3, \ldots, J$ [see Appendix A3 for $(\xi', \zeta')_j$].

As in the previous stability analysis, a low-order three term solution generates two unstable regions. The first region, $Z(t+2T)$, is identified by the $\cos\theta$ term in Equation (32) whereas the lowest order unstable region, $Z(t+4T)$, is identified by the period doubling term $\cos(\theta/2)$. Thus, the subharmonic Hill's equation suggests the possible cascade of period doubling. If the period doubling sequence is infinite, the resulting motion is chaotic (Thompson and Stewart, 1986). Numerical simulation of system response identifies a $4T$ subharmonic which continues to double and become chaotic (Fig. 9). While the mT subharmonic repeats after m intervals, the chaotic attractor does not, consequently generating a fractal map. The chaotic attractor is also characterized by a continuous spectra showing its "random like" behavior.

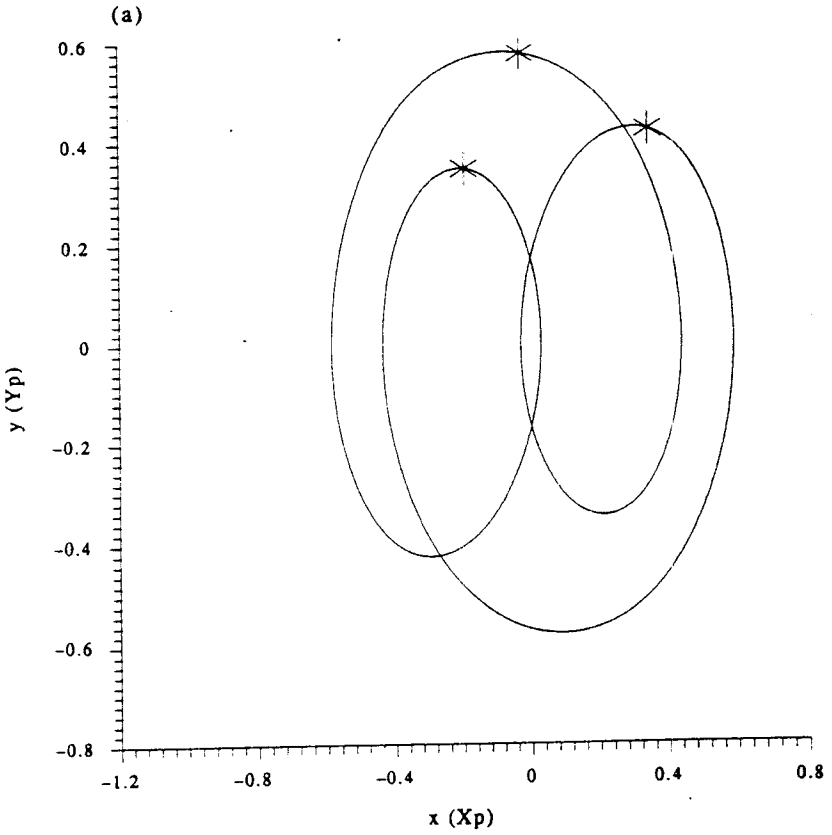

FIG. 10. Transient response near an explosion: (a) phase plane and Poincaré map, (b) Poincaré section. [(1) $3T$, (2) T.]

5.2. *Tangent explosions and transition states*

Numerical investigation of the transition states near the predicted tangent subharmonic bifurcations [Equation (20)] reveals lengthy transient solutions and sensitivity to initial conditions associated with the abrupt change from neighboring periodic motions. This route to chaos can be described by contraction of the mT subharmonic (see Figs 6 and 10, $m = 3$) that results in a chaotic attractor before settling to T periodic motion. The sharp transition does not always lead to a chaotic attractor, but appears as lengthy transients depicted by the Poincaré section $[N_P, X_P]$ which describe the evolution of the map from initial conditions to a final periodic or chaotic steady state (Fig. 10).

5.3. *Controlling mechanisms*

Investigation of the controlling mechanisms for the global bifurcations identified is performed by numerical investigation of the parameter set near the bifurcation values. Period doubling is found to be sensitive to the magnitude of the weak bias $[O(\mu\delta f^2)]$ generated by the nonlinear drag term. Comparison of these results to system response

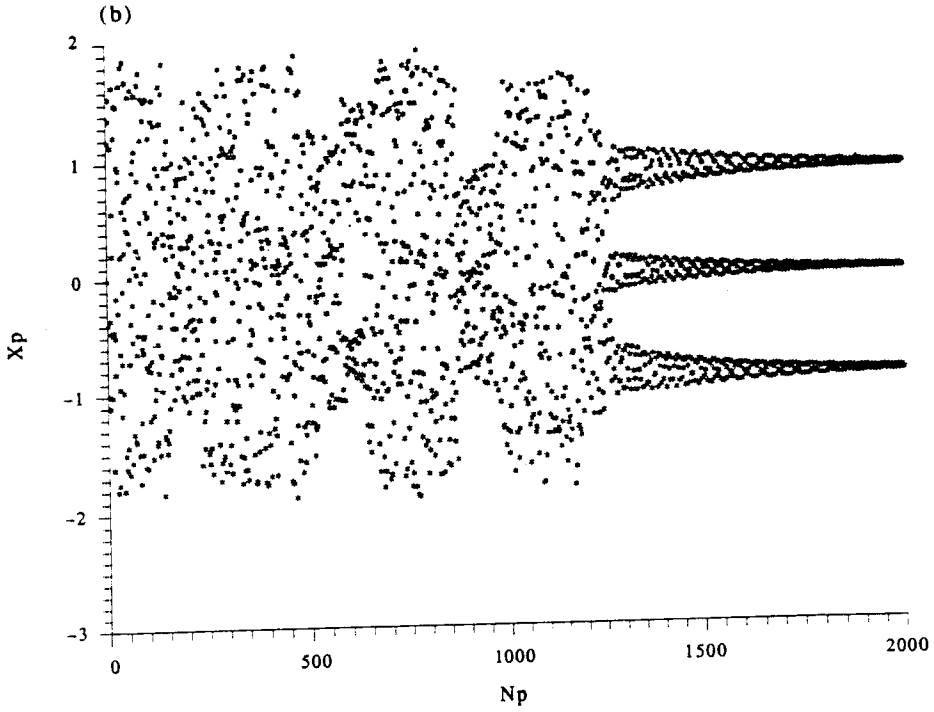

FIG. 10. (Continued).

in which the nonlinear drag was equivalently linearized [resulting in linear damping and change in phase to the harmonic excitation: Gottlieb (1991)] does not reveal the subharmonic instabilities. Consequently, equivalent linearization of the hydrodynamic drag force will not account for even subharmonic instabilities. The odd tangent instabilities are controlled by the nonlinear mooring force $[O(\alpha_{n>1})]$ and are only slightly modified by the parametric excitation $[O(\alpha\mu\delta f)]$. Furthermore, local period doubling and subharmonic tangent instabilities were found in a linearized mooring configuration. However, these instabilities were not found to be sensitive to initial conditions.

6. CLOSING REMARKS

Stability analysis of a multi-point mooring system in a drag-dominated environment is investigated. The system is shown to be globally stable for small excitation but reveals coexisting periodic solutions and sensitivity to initial conditions for larger excitation. Local and global bifurcations identifying routes to chaotic motions are determined semi-analytically. Controlling mechanisms of drag-induced instabilities and chaotic states are identified.

The system is characterized by a variable geometrically nonlinear restoring force and a coupled wave–structure exciting force consisting of quadratic drag and harmonic inertial components. The system, which incorporates the exact relative motion quadratic drag nonlinearity, was formulated to enable isolation and investigation of the influence of the nonlinear drag. The variable restoring force changes from a linear to a strongly

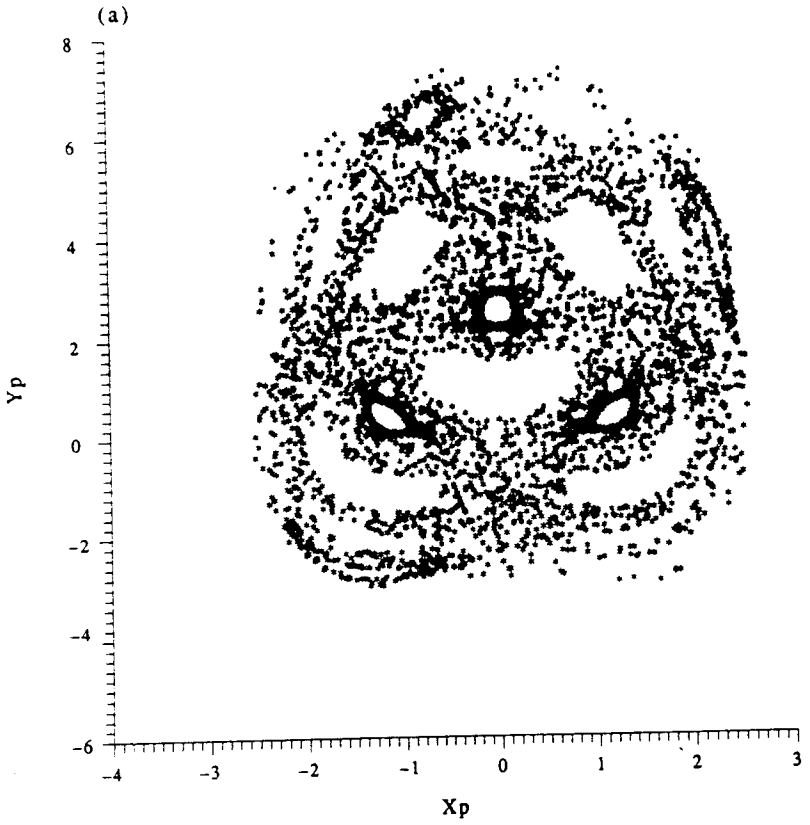

FIG. 10. (Continued).

nonlinear formulation and the drag force includes a bias, parametric excitation and a quadratic nonlinearity.

Two semi-analytic methods describing local and global bifurcations of the mooring system are derived and verified numerically. The methods incorporate stability analyses techniques from dynamical systems theory identifying local bifurcations which are further investigated numerically to determine existence of global bifurcations and chaotic states. The first method consists of formulating and investigating the stability of a corresponding Poincaré map and is used for analysis of near-resonant tangent bifurcations. The second method assumes nonresonant solution forms and investigates their stability by a variational approach in order to obtain period doubling phenomena.

Two routes to chaotic motion evolving from the subharmonic period doubling and tangent bifurcations are identified. The first is a continuous route via a period doubling cascade, whereas the second is abrupt and is accompanied by lengthy transients. The controlling mechanism found for the period doubling is the weak bias $[O(\mu\delta f^2)]$ generated by the nonlinear drag term, whereas the odd tangent instabilities are controlled by the nonlinear mooring force $[O(\alpha_{n>1})]$ and are only slightly modified by the parametric excitation $[O(\mu\delta f)]$. Consequently, equivalent linearization of the hydro-

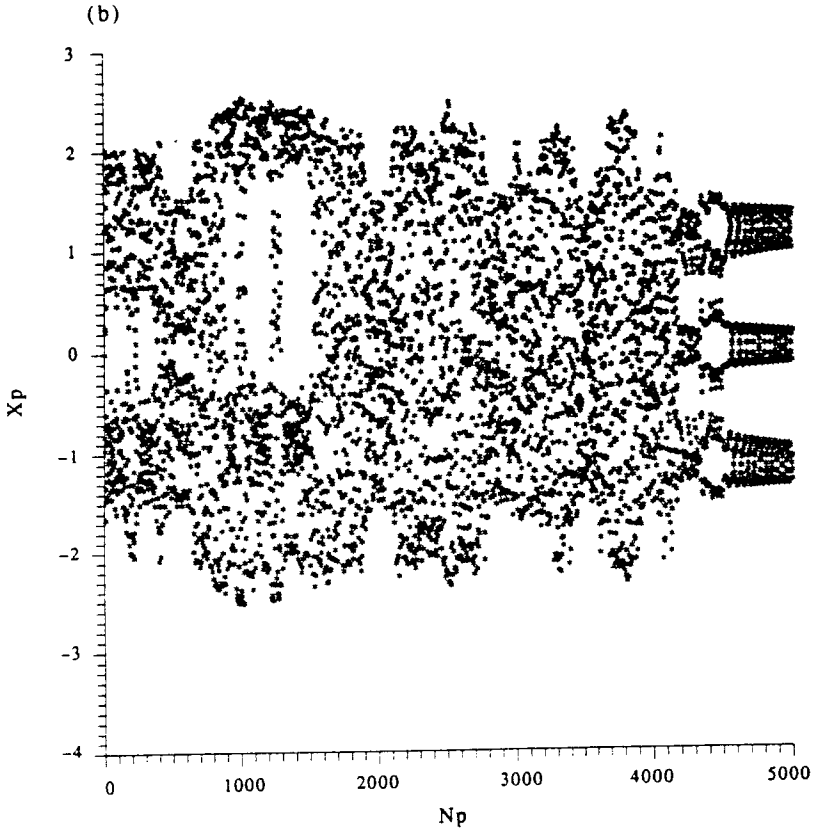

FIG. 10. (Continued).

dynamic drag force will not account for even subharmonic instabilities which need to be considered in the analysis of strongly nonlinear ocean mooring systems in a drag-dominated environment.

Acknowledgement—The authors gratefully acknowledge the financial support from the United States Office of Naval Research (grant No. N00014-88-K-0729).

REFERENCES

BERNITSAS, M.M. and CHUNG, J.S. 1991. Nonlinear stability and simulation of a two-line ship towing and mooring. *Appl. Ocean Res.* **11**, 153–166.

BISHOP, S.R. and VIRGIN, L.N. 1988. The onset of chaotic motions of a moored semi-submersible. *ASME J. Offshore Mech. Arctic Engng* **110**, 205–209.

CHOI, H.S. and LOU, Y.K. 1991. Nonlinear behavior of an articulated offshore loading platform. *Appl. Ocean Res.* **13**, 63–74.

GOTTLIEB, O. 1991. Nonlinear oscillations, bifurcations and chaos in ocean mooring systems. Ph.D. thesis, Oregon State University, U.S.A.

GOTTLIEB, O. 1992. Bifurcations and routes to chaos in wave–structure interaction systems. *AIAA J. Guidance, Control and Dynamics* (in press).

GOTTLIEB, O. and YIM, S.C.S. 1992. Nonlinear oscillations, bifurcations and chaos in a multi-point mooring system with a geometric nonlinearity. *Appl. Ocean Res.* (in press).

GOTTLIEB, O., YIM, S.C.S. and HUDSPETH, R.T. 1992. Analysis of nonlinear response of an articulated tower. *ISOPE J. Offshore Polar Engng* (in press).
GUCKENHEIMER, J. and HOLMES, P. 1986. *Nonlinear Oscillations, Dynamical Systems and Bifurcation of Vector Fields*. Springer, New York.
HAYASHI, C. 1964. *Nonlinear Oscillations in Physical Systems*. McGraw-Hill, New York.
HOLMES, P.J. 1980. Averaging and chaotic motions in forced oscillations. *SIAM J. appl. Math.* **38**, 65–80.
IOOS, G. and JOSEPH, D.D. 1981. *Elementary Stability and Bifurcation Theory*. Springer, New York.
JIANG, T. 1991. Investigation of nonlinear ship dynamics involving stability and chaos in examples from offshore technology. Institut für Schiffbau der Universitat Hamburg, Report No. 512 (in German).
LIAW, C.W. 1988. Chaotic and periodic responses of a coupled wave–force and structure system. *Computers Structures* **30**, 985–993.
MILES, J.W. 1988. Resonance and symmetry breaking for the pendulum. *Physica D* **31**, 252–268.
NAYFEH, A.H. and KHDEIR, A.A. 1986. Nonlinear rolling of ships in regular beam seas. *Int. Shipbldg Prog.* **33**, 40–49.
NAYFEH, A.H. and MOOK, D.T. 1979. *Nonlinear Oscillation*. Wiley, New York.
NEWMAN, J.N. 1977. *Marine Hydrodynamics*. MIT Press, Cambridge, Massachusetts.
PAPOULIAS, F.A. and BERNITSAS, M.M. 1988. Autonomous oscillations, bifurcations and chaotic response of moored vessels. *J. Ship Res.* **32**, 220–228.
SALAM, F.M.A. and SASTRY, S.S. 1985. Dynamics of the forced Josephson circuit: the regime of chaos. *IEEE Trans. Cir. Syst.* **32**, 784–796.
SANDERS, J.A. and VERHULST, F. 1985. *Averaging Methods in Nonlinear Dynamics*. Springer, New York.
SARPKAYA, T. and ISAACSON, M. DE ST Q. 1981. *Mechanics of Wave Forces on Offshore Structures*. Van Nostrand Reinhold, New York.
SHARMA, S.D., JIANG, T. and SCHELLIN, T.E. 1988. Dynamic instability and chaotic motions of a single-point moored tanker. *Proceedings of the 17th ONR Symposium on Naval Hydrodynamics*, pp. 543–563.
SZEMPLINSKA-STUPNICKA, W. 1987. Secondary resonances and approximate models of routes to chaotic motions in nonlinear oscillators. *J. Sound Vibr.* **113**, 155–172.
THOMPSON, J.M.T., BOKAIAN, A.R. and GHAFFARI, R. 1984. Subharmonic and chaotic motions of compliant offshore structures and articulated mooring towers. *J. Energy Resources Tech.* **106**, 191–198.
THOMPSON, J.M.T. and STEWART, H.B. 1986. *Nonlinear Dynamics and Chaos*. Wiley, Chichester.
TROGER, H. and HSU, C.S. 1977. Response of a nonlinear system under combined parametric and forcing excitation. *ASME J. appl. Mech.* **44**, 179–181.
WITZ, J.A., ABLETT, C.B. and HARRISON, J.H. 1989. Nonlinear response of semi-submersibles with nonlinear restoring moment characteristics. *Appl. Ocean Res.* **11**, 153–166.
YAGASAKI, K., SAKATA, M. and KIMURA, K. 1990. Dynamics of a weakly nonlinear system subjected to combined parametric and external excitation. *ASME J. appl. Mech.* **57**, 209–217.

APPENDIX

A1. Amplitude equations [Equation (23)]:

$$S_j(A_0, A_{ilm}, \Psi_{ilm}) = 0$$

where $I = 3$, $M = 1$: $\theta = A_0 + A_1\cos(\omega t + \Psi_1)$

$$R_0^2 + \frac{1}{2}(R_{1S}^2 + R_{1C}^2 + R_{2C}^2 + R_{3C}^2) - \frac{3}{8}(\mu\delta)^2(S_{4C}^2 + S_{4S}^2) = 0$$

$$2R_0R_{1C} + R_{2C}(R_{1C} + R_{3C}) = 0 \qquad \text{(A1a)}$$

$$2R_0R_{1S} - R_{1S}R_{2C} = 0$$

$$R_0 = \alpha_1 A_0 + \alpha_3\left(A_0^3 + \frac{3}{2}A_1^2\right)$$

$$R_{1C} = (\alpha_1 - \omega^2)A_1 + 3\alpha_3\left(A_0^2A_1 + \frac{1}{4}A_1^3\right) + \mu\omega^2 f\sin\Psi_1$$

$$R_{1S} = -\omega\gamma A_1 - \mu\omega^2 f\cos\Psi_1 \qquad \text{(A1b)}$$

$$R_{2C} = \frac{3}{2}\alpha_3 A_0 A_1^2$$

$$R_{3C} = \frac{1}{4}\alpha_3 A_1^3$$

$$S_C = f\cos\Psi_1 \tag{A1c}$$

$$S_S = f\sin\Psi_1 + A_1.$$

A2. Coefficients for harmonic variational system [Equation (28)]:

$$\xi_{C1} = f + A_1\sin\Psi_1 \tag{A2a}$$

$$\xi_{S1} = A_1\cos\Psi_1$$

$$\zeta_0 = \alpha_1 + \frac{3}{2}\alpha_3(2A_0^2 + A_1^2)$$

$$\zeta_{C1} = 6\alpha_3 A_0 A_1\cos\Psi_1$$

$$\zeta_{S1} = 6\alpha_3 A_0 A_1\sin\Psi_1 \tag{A2b}$$

$$\zeta_{C2} = \frac{3}{2}\alpha_3 A_1^2\cos 2\Psi_1$$

$$\zeta_{S2} = \frac{3}{2}\alpha_3 A_1^2\sin 2\Psi_1.$$

A3. Coefficients for harmonic variational system [Equation (32)]:

$$\xi_{C/2} = \frac{1}{2}A_{1/2}\sin\Psi_{1/2}$$

$$\xi_{S/2} = \frac{1}{2}A_{1/2}\cos\Psi_{1/2} \tag{A3a}$$

$$\xi_{C1} = f + A_1\sin\Psi_1$$

$$\xi_{S1} = A_1\cos\Psi_1$$

$$\zeta_0 = -\alpha_1 - \frac{3}{2}\alpha_3(2A_0^2 + A_{1/2}^2 + A_1^2)$$

$$\zeta_{C/2} = -3\alpha_3[2A_0A_{1/2}\cos\Psi_{1/2} + A_{1/2}A_1\cos(\Psi_1 - \Psi_{1/2})]$$

$$\zeta_{S/2} = 3\alpha_3[2A_0A_{1/2}\sin\Psi_{1/2} + A_{1/2}A_1\sin(\Psi_1 - \Psi_{1/2}] \tag{A3b}$$

$$\zeta_{C1} = -3\alpha_3\left[\frac{1}{2}A_{1/2}^2\cos(2\Psi_{1/2}) + 2A_0A_1\cos\Psi_1\right]$$

$$\zeta_{S1} = 3\alpha_3\left[\frac{1}{2}A_{1/2}^2\sin(2\Psi_{1/2}) + 2A_0A_1\sin\Psi_1\right].$$